Raman investigation of damage caused by deep ion implantation in diamond

J. O. Orwa, K. W. Nugent, D. N. Jamieson, and S. Prawer*
School of Physics, University of Melbourne, Parkville, Victoria, 3052, Australia
(Received 9 December 1999)

Raman microscopy has been employed to investigate the nature of damage created when natural type-IIa diamond is irradiated with MeV alpha particles. Three features appear in the Raman spectrum due to damage, viz., (i) the first-order diamond Raman line is broadened and downshifted, (ii) broad features appear which are a measure of the vibrational density of states of ion-beam-amorphized diamond, and (iii) the damage causes the appearance of sharp defect-induced Raman peaks at 1490 and 1630 cm^{-1}. For damage below an amorphization threshold, a linear relationship exists between the full width at half maximum and frequency shift, which shows that these are Kramers-Kronig related. The annealing behavior of the sharp Raman feature at 1490 cm^{-1} suggests that this peak is associated with vacancies with an activation energy for annealing of 4.06 eV, while the 1630-cm^{-1} peak is due to an interstitial related defect with an activation energy of 1.2 eV. For sub-MeV ion irradiation, damage beyond the critical amorphization level usually leads to relaxation of the diamond structure to graphite upon thermal annealing. However, for MeV ion irradiation, it was found that annealing, even when the ion induced damage level is well above the amorphization threshold, could restore the original diamond structure. We attribute this result to the high internal pressure the damaged layer is subjected to which does not allow relaxation to graphitically bonded structures.

I. INTRODUCTION

Diamond, because of its unique physical and chemical properties,[1] is an ideal material for specialized applications in electronics compared to widely used materials such as silicon. Diamond is a wide bandgap semiconductor, and thus its electrical behavior at room temperature largely resembles an insulator. As with most semiconductors, the electronic properties in diamond can be improved by adding dopants. An attractive method for doping diamond is ion implantation.[2] The drawback is that ion implantation introduces defects which must be repaired to realize the envisaged superior electronic properties. Residual defects are responsible for trapping and compensation which degrade the electrical behavior and limit realization of electronic grade doped diamond (particularly *n* type).

Raman spectroscopy has long been used to study carbons because of its ability to sensitively distinguish carbon allotropes.[3,4] In a recent report,[5] we showed that Raman spectroscopy is extremely sensitive to the damage created by ion irradiation. One particular defect which gives rise to a peak at 1490 cm^{-1} in the Raman spectrum of ion-irradiated diamond was found to be strongly correlated with the compensation of carriers in *p*-type diamond. When this defect was removed by thermal annealing, very high mobility *p*-type diamond (hole mobility$=600$ $cm^2/V\,s$ with a low compensation ratio of about 5%) could be fabricated. Hence there is a strong motivation for studying the evolution and thermal annealing of defects in diamond as part of the overall effort to optimize diamond for electronic applications.

This paper presents a detailed Raman investigation of MeV radiation damage in diamond. We use cross-sectional Raman microscopy (described in Sec. II) to study the defects created as a function of damage density and annealing temperature. The motivation for using MeV ions is to create a damage layer deeply buried below the diamond surface with a relatively undamaged confining cap which keeps the damaged region under high pressure and thus restrains it from relaxing to graphite. The use of inert helium ions ensures that no chemical interaction occurs between the implanted species and the substrate so that any features observed are purely due to damage.

A. Ion-beam-induced damage in diamond

Energetic ions incident on the surface of a solid will penetrate and come to rest at a distance determined by the ion energy, ion mass, and properties of the target material. The passage of an ion creates a collision cascade, which is well described by simulation programs such as transport of ions in matter (TRIM) code.[6] This passage breaks many bonds, creating many defects along the ion track, which can aggregate: thus the damaged material can be rich in both point and more complex defects such as dislocations. Diamond, like other covalently bonded semiconductors, will amorphize once the damage level exceeds a critical density. For Si and Ge, thermal annealing results in recrystallization of the lattice. However, the situation is more complicated for diamond because its structure is metastable with respect to graphite, and transformation to the latter is a common occurrence during irradiation or following post-implantation heat treatment.

The processes of ion beam modification and thermal annealing of diamond have been extensively reviewed.[7–11] The macroscopic manifestations of the damage, which are associated with the transformation from sp^3 to sp^2 bonding, include very large increases in electrical conductivity, chemical etchability, increased Rutherford backscattering spectroscopy (RBS) dechanneling and reduction in $\chi_{\min}$, and discoloration. Most studies have focused on ion-beam-induced damage close to the surface such as created by sub-MeV light ions. For this near surface damage, a critical damage level of 1×10^{22} vac cm^{-3},[12] referred to as D_c, has been

identified above which the diamond structure amorphizes and cannot be restored by annealing. It is not established whether this critical level applies to deeply buried damage as well.

While the macroscopic changes which occur in ion-irradiated diamond are known, the microscopic nature of the damage is not clear, partially due to the absence of detailed transmission electron microscopy (TEM) studies of ion-irradiated diamond. One attempt at a microscopic model[13] based on the model of Morehead and Crowder envisages that the passage of each ion leaves a ''trail'' of damaged spheres of average radius r. In the case of ion irradiation of silicon, these spheres are primarily comprised of amorphous silicon. When this model is applied to diamond, each sphere is envisaged to consist of partially graphitized material. The electrical conductivity and size of each of these spheres depend largely on the implantation temperature. When the concentration of these spheres reaches a sufficient level, a connective pathway may be formed between them resulting in a very sharp rise in conductivity as is observed.[14] The damage level at which this overlap occurs is also very close to the damage level above which sub-MeV ion-irradiated diamond collapses to graphite upon thermal annealing and the damage level at which RBS and other measurements indicate that the diamond lattice has been ''amorphized.'' Despite the success of this model, no direct evidence has been produced to confirm the existence of islands of amorphized and graphitized clusters in ion-beam-irradiated diamond.

B. Raman spectroscopy of ion-irradiated materials

The effect of ion implantation on covalent materials is characterized by Raman spectroscopy using the phonon confinement model,[15] which has been used to explain the skewing and downward shift of the first-order Raman line as the damage level increases. Normally, momentum conservation limits the Raman scattering to the zone center phonon (i.e., $q=0$). However, if the phonons are confined in space by microscrystallite boundaries or defects, there will be uncertainty in the phonon momentum, allowing phonons with $q>0$ to contribute to the Raman signal. For example, skewing of the first-order Raman peak in silicon at 520 cm^{-1}, indicative of phonon confinement, has been observed for doses as small as 1×10^{11} Si cm^{-2}. The exact shape of the Raman line depends on the details of the phonon dispersion curve close to the zone center.

At damage levels approaching or exceeding the amorphization limit, the Raman spectrum reflects the vibrational density of states (VDOS) integrated over all modes and all frequencies. As the translational symmetry, which characterizes the crystalline structure, is lost, the optical vibrations are localized instead of extending in the total periodic crystal. If the coherence length between optical vibrations is too small, the Raman spectrum is basically the broadened phonon density of states. (For silicon this occurs when the cluster size is of the order of 10 interatomic spacings or less.) The Raman intensity can then be expressed as[16]

$$I(\omega)=\sum_b (C_b/\omega)[1+n(\omega)]g_b(\omega), \tag{1}$$

where $g_b(\omega)$ is the VDOS, $1+n(\omega)$ is the thermal population of the initial states, and the constant C_b depends on the band b. For a-Si a broad, but well-defined peak is observed at about 480 cm^{-1} in excellent agreement with the VDOS as measured by neutron scattering. For silicon damaged at an intermediate level, the Raman spectrum consists of a mixture of a skewed Lorentzian crystalline silicon peak and an amorphous silicon peak. This is consistent with the Morehead-Crowder model in which amorphous Si clusters are created along the ion track. The ratio of the intensity of the a-Si peak to the c-Si peak can then be used to define an amorphous fraction.

In contrast with Si, as will be seen below, the Raman signal shows evidence for the presence of amorphized diamond for even the lowest damage levels studied. Furthermore, for higher doses, despite the presence of the amorphous component, no corresponding skewing of the first-order diamond line is observed even when down shifted by up to 50 cm^{-1}. In addition, very sharp peaks appear in the Raman spectrum at 1490 and 1630 cm^{-1}, which, in some cases, have a full width at half maximum (FWHM) less than that of the first-order diamond line.

C. Annealing kinetics

Defect annealing can result from one or a combination of processes. Simple defects can form defect complexes by combination whereas complex defects can dissociate to form simpler defects. In each case the concentration of the original defect diminishes as manifested by a decrease in the intensity of the monitored signal. Each process that results in the annealing of a defect is characterized by an activation energy, which the defect must have to initiate the annealing. The activation energy is easily extracted from the equations that describe the relevant annealing kinetics.

If a material consisting of N defects per unit volume is subjected to annealing, the rate of change in the number of defects is given by the differential equation

$$\frac{dN}{dt}=-r_\alpha N^\alpha, \tag{2}$$

where α is the order of the reaction: r_α is a temperature-dependent quantity called the rate constant and is related to the diffusion coefficient of the defect and, hence, the temperature. The rate constant is expressed as

$$r_\alpha=A\exp\left(-\frac{E_a}{k_BT}\right), \tag{3}$$

so that Eq. (2) can be solved for $\alpha=1$ and $\alpha=2$ to obtain

$$N(t)=N_0\exp(-r_1t) \tag{4}$$

and

$$N(t)=\frac{N_0}{1+N_0r_2t}, \tag{5}$$

respectively. In the preceding three equations, A is a constant which contains the vibrational frequency associated with the process[17] and N_0 is the defect concentration at time $t=0$.

To obtain the activation energy, one may perform isothermal or isochronal annealing. We performed isochronal annealing for which, in the case of $\alpha=1$, Eqs. (2) and (3) can be combined and solved to yield[17,18]

$$N=N_0\exp\left[-\frac{Ak_BT^2}{E_a}\exp\left(-\frac{E_a}{k_BT}\right)\right], \tag{6}$$

where A has the same meaning as in Eq. (3). By treating E_a and A as adjustable parameters, experimental data on the intensity of the various peaks as a function of the annealing temperature can be fitted to Eq. (6) to obtain the activation energy.

II. EXPERIMENT

The sample studied was a natural type-IIa diamond slab of dimensions $(3\times3\times0.5)$ mm from Drukker Corporation, Netherlands. All faces of the diamond were polished with the main face a (100) plane and the edges parallel to the (010) and (001) crystal planes. The edge was implanted with 3-MeV alpha particles at room temperature in the random orientation to a dose of $1\times10^{17}\,\mathrm{cm}^{-2}$. The beam was delivered by the 5U pelletron accelerator at The University of Melbourne. The longitudinal range and range straggling of the helium ions was determined using TRIM as $R_p\pm\Delta R_p=5.88\pm0.25\,\mu$m.

The as-implanted diamond was oriented such that the [100] direction was parallel to the incident laser beam. Thus the laser beam was perpendicular to the original implantation direction, allowing cross-sectional sampling of the damaged region. A schematic diagram of the implantation and Raman analysis geometry employed is presented elsewhere.[19,21] The incident beam polarization was varied from $E_i\|[010]$ to $E_i\|[001]$, while the polarization of the scattered beam, E_s, was fixed parallel to [001]. Under these conditions, the first-order diamond Raman line at around 1332 cm^{-1} is allowed by the selection rules when E_i is parallel to [010] (i.e., the polarization of the input beam is perpendicular to the direction of the fixed polarization analyzer) and forbidden when E_i is parallel to [001] (i.e., the input beam polarization direction is parallel to the analyzer direction). The spectra obtained in the above configurations will be referred to as ''diamond allowed'' and ''diamond forbidden.''

The 514.5-nm line of an argon ion laser was the main excitation wavelength used although the 488-nm line was also used to distinguish between Raman and luminescence bands as well as to identify any resonance enhancement. The beam was focused to a 1-μm spot using a $\times100$ Olympus microscope objective. The backscattered light was collected through the same objective and was analyzed by a DILOR *XY* confocal micro-Raman spectrometer with optical multichannel collection using a charge coupled device (CCD) array detector.

Using a confocal aperture of 120 μm, a cylindrical region of about 1 μm diameter and 2 μm height was sampled in a typical measurement. Use of the cross-sectional Raman analysis geometry described earlier allowed the Raman spectra to be recorded at different depths below the implantation surface. Since the damage level increases with ion penetration depth, the analysis described provided a convenient and accurate way of profiling damage compared to the usual technique of directing the analysis beam along the original implantation direction.

According to the selection rules the diamond line at 1332 cm^{-1} should not be visible at all in the ''diamond-forbidden'' configuration. A small breakthrough in the diamond line was, however, observed in this orientation and is attributed to deviation from ideal backscatter geometry of the scattered light due to the large numerical aperture of the objective used. Correction for the breakthrough in the two analysis orientations was achieved through the equations

$$N_{\mathrm{TFS}}=N_{\mathrm{MFS}}-(0.065\times3\times N_{\mathrm{MAS}}) \tag{7}$$

and

$$N_{\mathrm{TAS}}=N_{\mathrm{MAS}}-N_{\mathrm{TFS}}, \tag{8}$$

where ''TFS'' and ''TAS'' refer to true forbidden spectra and true allowed spectra, while ''MFS'' and ''MAS'' are measured forbidden spectra and measured allowed spectra, respectively. The factor of 3 in Eq. (7) takes into account the difference in integration time between spectra collected in the two configurations, while the 0.065 is the ratio of the intensity of the first-order diamond line in ''diamond-forbidden'' orientation of a pristine diamond to that in ''diamond-allowed'' configuration. The sample was then subjected to 1 h annealing in flowing argon at successively higher temperatures between 373 and 1473 K. Each annealing was followed by the set of Raman measurements described above for the as-implanted sample.

III. EXPERIMENTAL RESULTS AND DISCUSSION

In this three-part presentation, we begin by studying the damage-induced structural modification of the diamond by following the changes in the first-order diamond line width and frequency as a function of depth. These changes occur as a result of the transition from an intact diamond structure with single isolated point defects close to the implantation surface to a disordered material near the end of range. The second part identifies the nature of the damage created following implantation and studies its subsequent annealing behavior by monitoring the intensity of the defect Raman peaks as a function of temperature. Finally, we discuss the annealing behavior of diamond, which has been completely amorphized by the ion irradiation, and show that under certain conditions this material will anneal back to diamond and not graphitize.

A. Structure of the zone center diamond peak as a function of the implantation depth

Undamaged diamond displays a single first-order Raman line at 1332 cm^{-1} and no other peaks in the range between 0 and 2000 cm^{-1}. When the diamond is damaged such as by ion beam irradiation, several other peaks appear in this range, most notably at 1490 and 1630 cm^{-1}. The Raman spectra obtained in the ''diamond-allowed'' and ''diamond-forbidden'' configurations are displayed in Figs. 1 and 2. The spectra of Fig. 1 have not been corrected for the 6.5% breakthrough, while those of Fig. 2 have been corrected to emphasize the damage peaks. The skewed appearance of the first-order diamond peak observed in Fig. 1 disappears once the

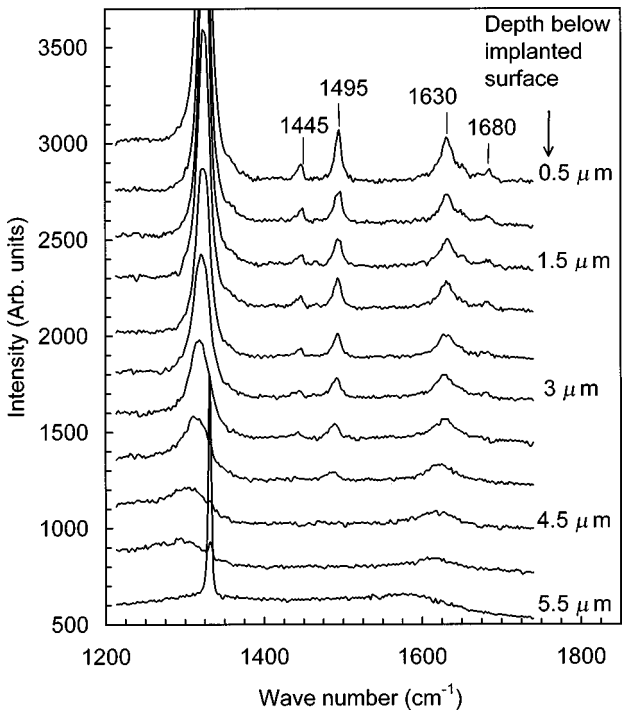

FIG. 1. ''Diamond-allowed'' spectra showing the first-order diamond peak and the damage peaks located at ~1450, 1490, 1630, and 1680 cm^{-1}. The spectra have been vertically displaced by about 250 units for clarity. The spectrum, which corresponds to the depth of 5.5 μm, represents the zero value for the traces.

spectra are corrected so that the peak can be fitted with just one Lorentzian as shown in the inset to Fig. 3 for a spectrum taken at a depth of 2 μm below the implanted surface. Figure 3 shows the FWHM and peak position extracted from such fits as a function of depth. The decrease in the intensity of the first-order diamond peak with depth (damage), evident in Fig. 1, is accompanied by a shift to lower wave numbers and a smooth linewidth broadening. The peak width varied from 13.3 cm^{-1} at a depth of 0.5 μm to 87.8 cm^{-1} at a depth of 5.0 μm. Over the same depth range, the peak position varied from 1325.8 to 1297.7 cm^{-1}. These parameters are compared with a peak width of 3.09 cm^{-1} centered at 1332.03 cm^{-1} for pristine diamond obtained under the same measurement conditions.

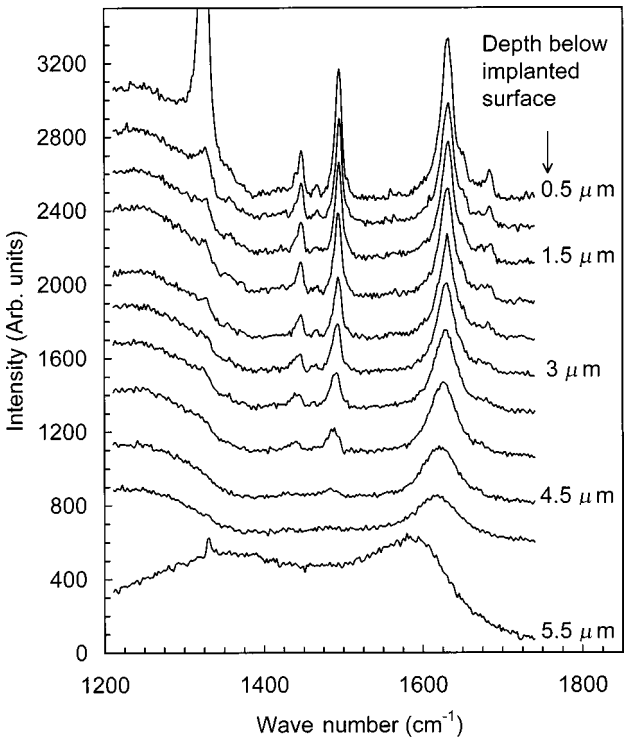

FIG. 2. ''Diamond-forbidden'' spectra showing much more pronounced damage peaks compared to corresponding spectra of Fig. 1 obtained in the ''diamond-allowed'' configuration. No base line has been subtracted, but the traces have been vertically displaced by a factor of about 200 for clarity.

Despite these large increases in peak width and shift with damage, the symmetric nature of the peak persisted for all depths below the surface except at the very end of range where the Raman spectrum is that of an amorphous material and no first-order peak can be observed. That the highly shifted and enormously broadened peak was still the first-order diamond peak was ascertained by the polarization behavior of the peak, which was similar to the behavior of the peak in undamaged diamond.

The symmetry of the diamond line indicates that there is little or no phonon confinement. The results suggest that the increase in the FWHM is due to a decrease in phonon lifetime as a result of scattering from the ion-induced defects. When a phonon decays, the zone center unperturbed frequency ω_0 undergoes a complex shift, $\Delta\omega + i\Gamma$. The real part redshifts the normal mode frequency and the imaginary part, which is the reciprocal of the phonon lifetime (usually referred to as the linewidth), increases. In the anharmonic approximation (which has been found to be applicable to diamond) the real and imaginary shifts should be linearly related to each other via Kramers-Kronig relationships.[20] Thus as the level of damage increases one expects the phonon lifetime to decrease, the FWHM to therefore increase, and (via Kramers-Kronig relationships) the peak position to be redshifted. Indeed, when the FWHM is plotted against the peak position, as shown in Fig. 4, a linear relationship exists over a wide range of frequencies (1331 to ~1312 cm^{-1}) and corresponding linewidths (4 to ~45 cm^{-1}). Outside this range, the FWHM and peak shifts are still Kramers-Kronig related, but the slope of the line changes. This change in slope corresponds to the damage level at which amorphization of the diamond lattice occurs. The linear dependence of the FWHM on peak shift indicates that the increase in the FWHM is a direct measure of the decrease in phonon lifetime and should be linearly related to defect density, provided the defects are isolated.

Plotting the FWHM and peak position versus the damage production as estimated by TRIM can further elucidate the role of damage. The projected end of range of 5.88 μm predicted by TRIM is about 0.5 μm deeper than the depth at which maximum damage occurs as determined by experiment from the first-order diamond line shift and from optical microscopy. Therefore, in constructing Fig. 5, the TRIM profile has been adjusted so that the peak damage coincides with the maximum peak shift at the same depth. It was also necessary to average the TRIM data over 0.5-μm intervals to match the spatial resolution of the Raman measurements.

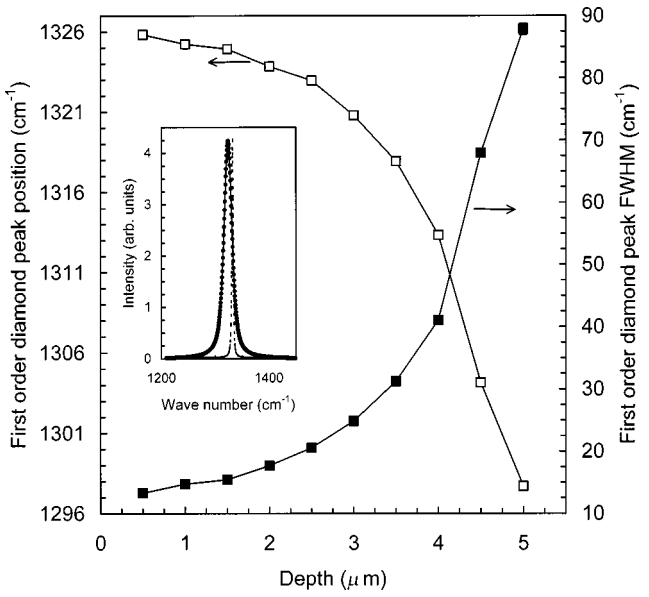

FIG. 3. Variation of the first-order diamond Raman peak position and FWHM with depth for 2 MeV, $1\times10^{17}\,\mathrm{cm}^{-2}$ carbon implanted, but unannealed diamond. The error for both the FWHM and peak position was of the order of the size of the symbols used to designate the data points. The inset is the first-order diamond Raman peak at $\sim$1330 cm^{-1} taken at a depth of 2 μm below the surface. The solid squares in the inset are data points, while the solid line is a single Lorentzian fit to the data points. The dotted curve is a spectrum from pristine diamond, shown here for comparison. The pristine diamond spectrum has been divided by 8000 to fit into the scale of the damaged diamond spectrum.

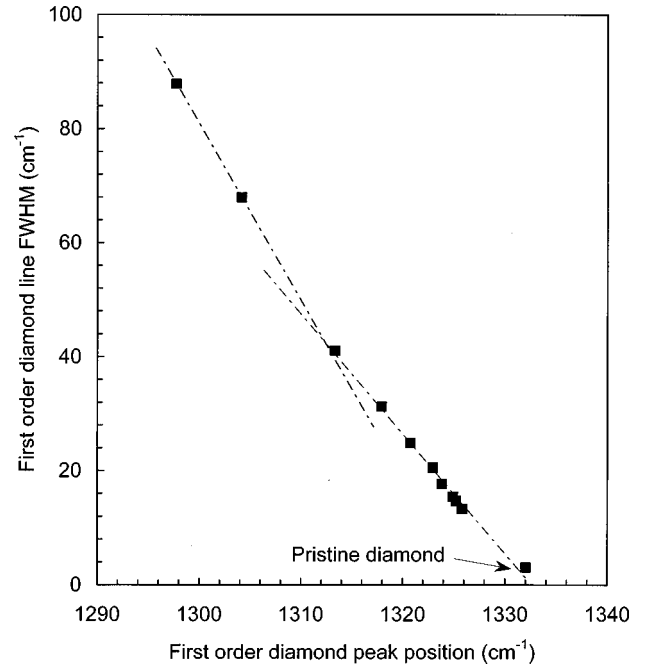

FIG. 4. Variation of the first-order diamond peak FWHM with peak position. The two lines correspond to regions with different levels of damage. The line with smaller linewidths corresponds to low levels of damage where the defects occur as isolated point defects. The other line represents higher levels of damage where the defects begin to overlap.

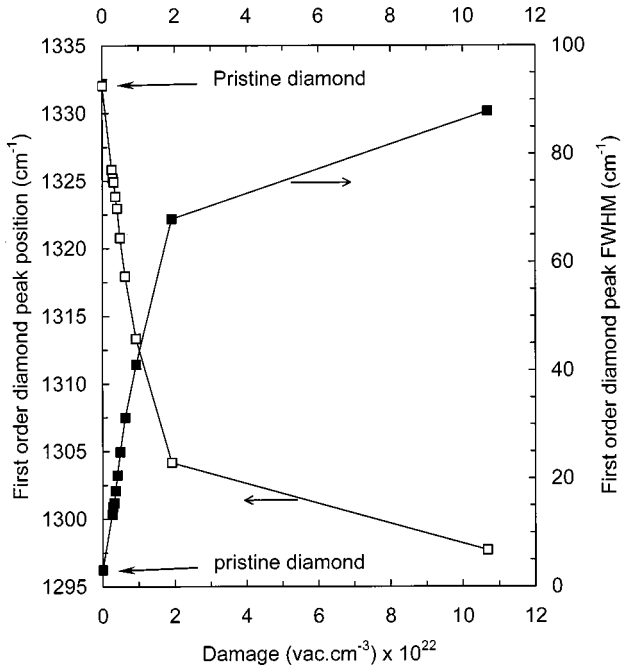

FIG. 5. First order diamond peak position and FWHM vs damage. The damage data were obtained from TRIM with $E_d=50$ eV.

Figure 5 shows that both the peak shift and FWHM exhibit a linear dependence on damage below a damage level of 1×10^{22} vac cm^{-3}. Above this damage level, the FWHM and peak position begin to saturate. This suggests that at this damage level the defects overlap to create a continuous amorphous layer. In Fig. 2 the Raman spectrum corresponding to this damage level (at 4.5 μm) shows no evidence of the presence of a first-order diamond line and is typical of the Raman spectrum from an amorphized material.

As mentioned earlier, for sub-MeV ion irradiation, there exists a critical damage level of about 1×10^{22} vac cm^{-3} above which the diamond structure amorphizes and cannot be restored by annealing. Annealing, under such circumstances, results in the collapse of the matrix to the more stable form of carbon, viz., graphite. The difference between sub-MeV and MeV ion damage is that for the latter, the damage is deeply buried underneath a large, relatively intact, diamond cap layer which keeps the damaged region under high pressure. The results of Fig. 5 suggest that a critical damage level of about 1×10^{22} vac cm^{-3} for amorphization is also applicable to deep ion implantation. However, as shown below, the high pressure, which exists due to the large constraining cap, prevents the amorphized layer from relaxing to graphite upon thermal annealing.

If indeed amorphous regions were formed along each ion track, one would expect to observe a signal from these regions, which closely follows the VDOS as per Eq. (1). Figure 6 shows normalized Raman spectra taken in the forbidden orientation (these spectra have not been corrected for polarization leakage and hence show a low-intensity first-order diamond line in some of the spectra close to the surface where the damage level is lowest). In addition to the various sharp peaks, the Raman spectrum of radiation-damaged diamond is characterized by broad skewed peaks centered at about 350 and 1245 cm^{-1}. The shapes of these broad features conform closely to the VDOS of diamond.[21] An esti-

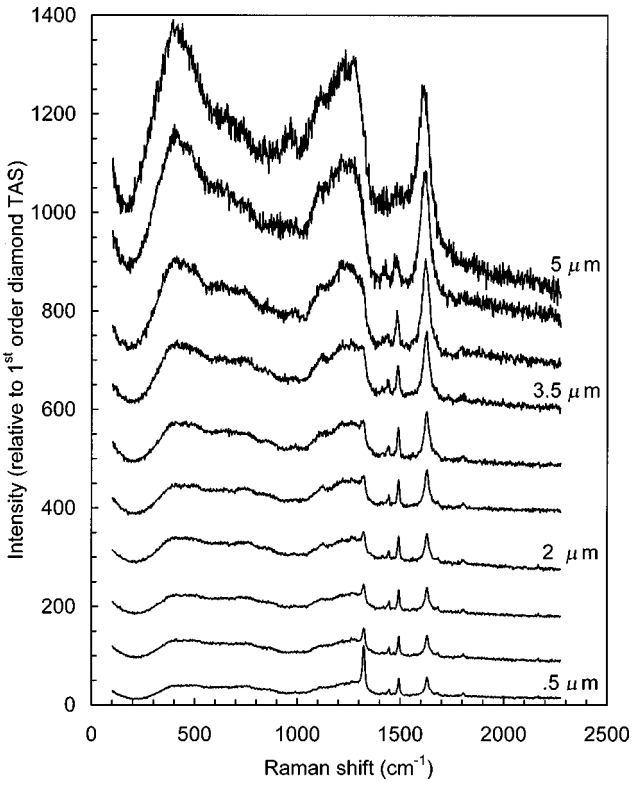

FIG. 6. Normalized Raman spectra as a function of depth (damage) showing the growth of the amorphous peak with increasing damage.

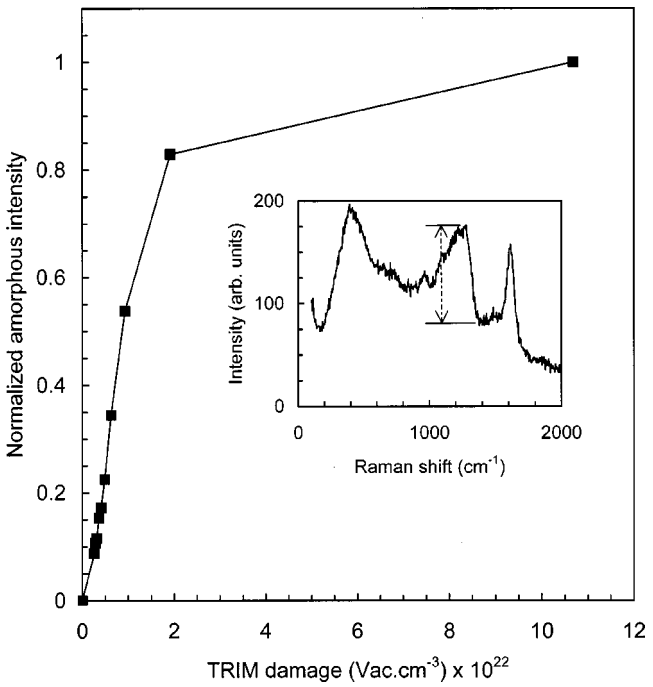

FIG. 7. Amorphous intensity vs TRIM damage showing that amorphous intensity is linear with damage up to a damage level of around 1×10^{22} vac/cm^3. The double arrow in the inset shows how the amorphous intensity was measured.

mate of the intensity of this amorphous component can be obtained by measuring the step height at 1245 cm^{-1} with respect to the background intensity at 1400 cm^{-1}. Figure 6 shows that, in the region of low damage where the damage occurs as isolated point defects, and away from the end of range, the amorphous peak coexists with the zone center phonon. Figure 7 is a plot the amorphous fraction normalized to unity at the maximum damage level (the inset of the same figure shows how the amorphous intensity was estimated). This amorphous fraction is the ratio of the amorphous intensity to that of the first-order diamond line in the irradiated region. Indeed, Fig. 7 shows that the amorphous fraction increases linearly with damage up to a damage level of $\sim1\times10^{22}$ vac cm^{-3}. Parameters such as the first-order diamond peak shift and FWHM which vary linearly with damage should also therefore vary linearly with the amorphous fraction as is indeed demonstrated in Fig. 8.

B. Defect-related peaks

Figure 2 shows the presence of sharp peaks at 1490 and 1630 cm^{-1} following ion irradiation. A number of smaller peaks are also observed at 1450, 1680, and 1800 cm^{-1}. To extract quantitative information from the spectra, the peaks at 1490 and 1630 cm^{-1} were fitted with a combination of Lorentzians and Gaussians. Figure 9 shows that the peak positions shift to lower wave numbers with increasing damage in an almost linear fashion below a damage level of about 1×10^{22} vac cm^{-3}, above which the peak shifts saturate. The inset in Fig. 9 shows the relationship between the FWHM and peak shift, which shows that the peak shifts are linearly related to the FWHM, consistent with a Kramers-Kronig relationship. Although the smaller peaks mentioned were not fitted, they showed behavior with damage and annealing temperature that was similar to the 1490-cm^{-1} peak as can be seen from Figs. 6 and 15. The 1490-cm^{-1} peak and the smaller peaks thus appear to belong to one family and may be caused by similar defects.

The intensity of the 1490- and 1630-cm^{-1} peaks, normalized with respect to the intensity of the diamond line in the

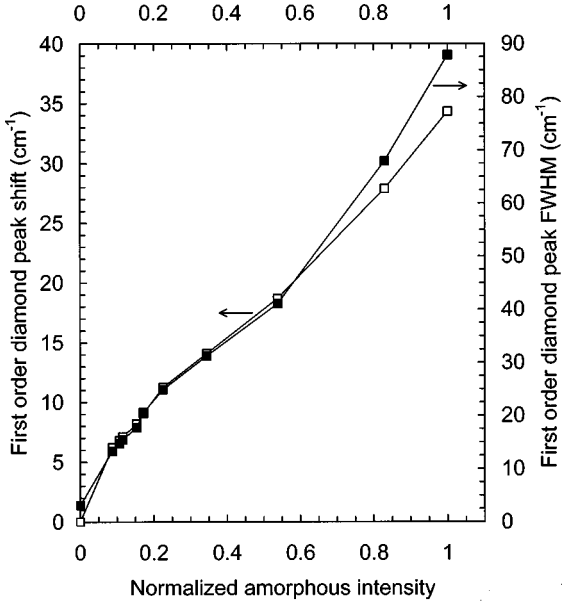

FIG. 8. The first-order diamond Raman peak shift and FWHM vs normalized amorphous intensity.

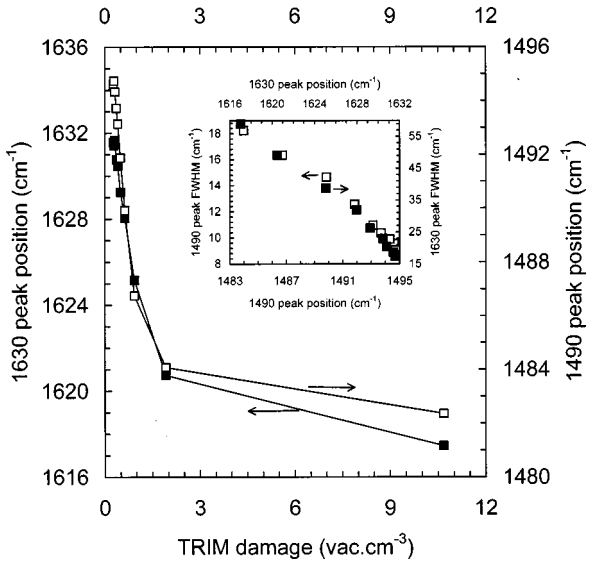

FIG. 9. The 1490-cm^{-1} (open squares) and 1630-cm^{-1} (solid squares) peak positions vs damage showing that the intensity of the peaks is linear with damage only for vacancy concentrations below 1×10^{22} cm^{-3}. The linear relationship between the defect peak positions and FWHM shown in the inset shows that the two are Kramers-Kronig related like the first-order diamond line.

''diamond-allowed'' configuration, varied with damage. However, the behavior was different for the two peaks. In Fig. 10 the intensity of the 1630-cm^{-1} peak increases linearly with damage up to about 1×10^{22} vac cm^{-3}, above which it saturates. By contrast, the intensity of the 1490-cm^{-1} peak jumps quickly to a maximum at a damage level of only $\sim4\times10^{21}$ vac cm^{-3} and stays fairly constant in the less damaged region close to the implanted surface, decreasing sharply when the damage level exceeds 7×10^{21} vac cm^{-3}. Above a damage level of

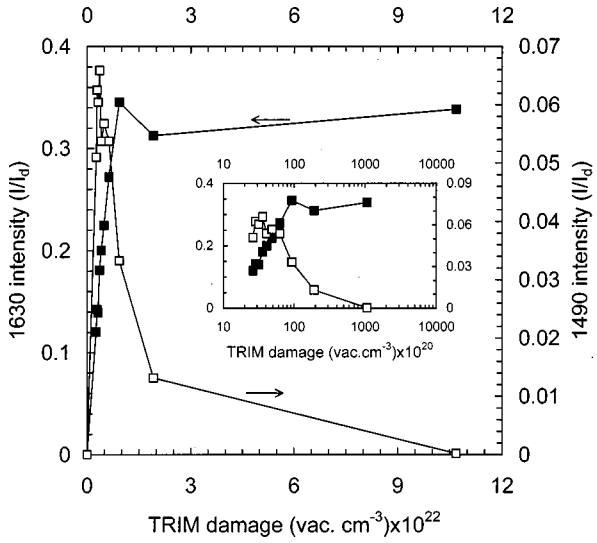

FIG. 10. The 1490- and 1630-cm^{-1} peak intensities vs TRIM damage. (I/I_d) in the vertical axis is the ratio of the intensity of the defect peak to the ratio of the intensity of the first-order diamond line measured at the same point. The inset shows the same plot with the x axis replaced by a logarithmic scale, while the other axes remain the same.

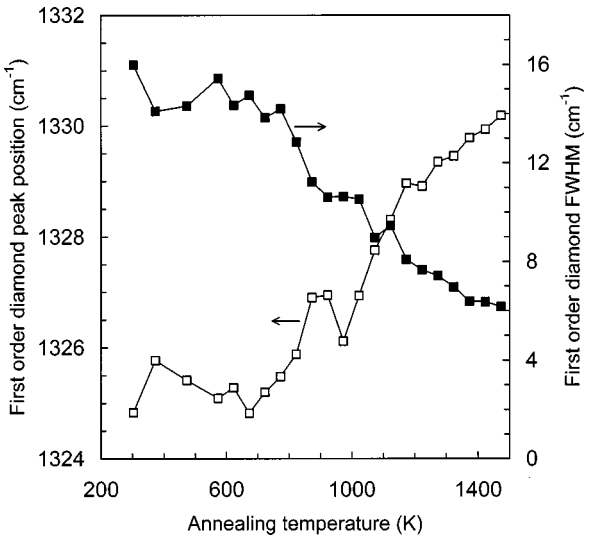

FIG. 11. The first-order diamond peak width and peak position averaged over the first 2 μm below the surface plotted against annealing temperature showing that the two are correlated.

$\sim6\times10^{22}$ vac cm^{-3}, the peak disappears. The inset of Fig. 10, where the TRIM damage has been plotted on a semilogarithmic scale, clearly shows the behavior of these peaks. The different dependence of the peaks on the level of damage makes it clear that the defects which give rise to the 1490- and 1630-cm^{-1} peaks have different origins.

Initial clues to the origins of these peaks can be obtained from their positions. Theoretical calculations on the VDOS of diamond[22] show that no states occur above 1400 cm^{-1} for sp^3-bonded carbon structures. The position of the 1490-cm^{-1} peak is roughly midway between the position of the vibrations due to the singly bonded diamond line at 1332 cm^{-1} and the graphitic double-bond modes at 1580 cm^{-1}. Thus the defect responsible for this peak is likely to consist of conjugated double and single bonds. On the other hand, the 1630-cm^{-1} peak most likely originates from some kind of C=C bond. Theoretical calculations[22] also suggest that modes above 1400 cm^{-1} are strongly localized. The observed sharpness of the peaks indicates that they originate from well-defined local rather than extended defects.

C. Annealing behavior

Annealing was performed for 1 h (this was sufficient time for annealing to reach equilibrium at each temperature) in flowing argon at several temperatures in the range 373–1473 K. In Fig. 11 the position of the first-order diamond line and FWHM are plotted as a function of annealing temperature for a point 2 μm below the surface (which corresponds to an initial defect density of 3.5×10^{21} vac cm^{-3}). A progressive upward shift in the first-order diamond Raman line position and a corresponding linewidth narrowing is observed as the temperature increases. After annealing at 1473 K, the first-order diamond line is at 1330.2 cm^{-1}, while the FWHM is 6 cm^{-1}. These values are to be compared with a shift of 1332.03 cm^{-1} and a FWHM of 3.09 cm^{-1} for pristine diamond, which indicates that some residual damage still remains at this annealing temperature. Figure 12 plots the peak position as a function of the FWHM for the temperature

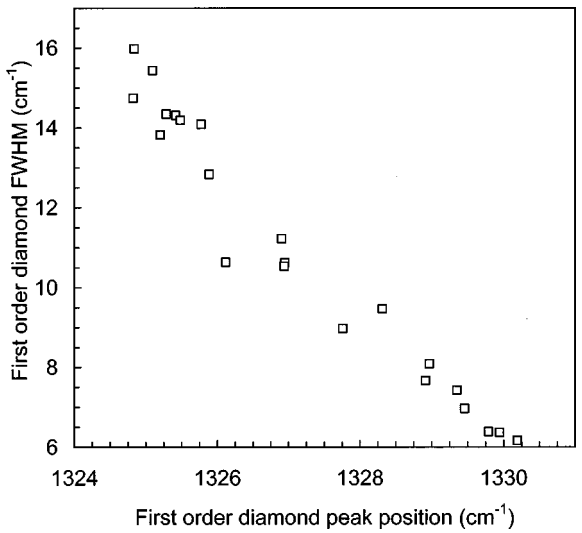

FIG. 12. Variation of the first-order diamond Raman peak position with FWHM in the temperature range 300–1470 K.

range 300–1473 K, which is well described by a single straight line. The existence of a simple linear dependence between the peak position and the FWHM indicates that the defects being removed by thermal annealing are those responsible for the scattering and decay of the zone center phonons as per the Kramers-Kronig relationship.

In Fig. 13 the amorphous fraction is plotted as a function of annealing temperature for both an initial damage level of 3.5×10^{21} vac cm^{-3} (i.e., a point 2 μm below the surface) and a damage level of 1.1×10^{23} vac cm^{-3} [i.e., at a point near the end of range (EOR)]. As expected for a point close to the surface with a defect density well below D_c, the amorphous fraction decreases as a function of annealing temperature.

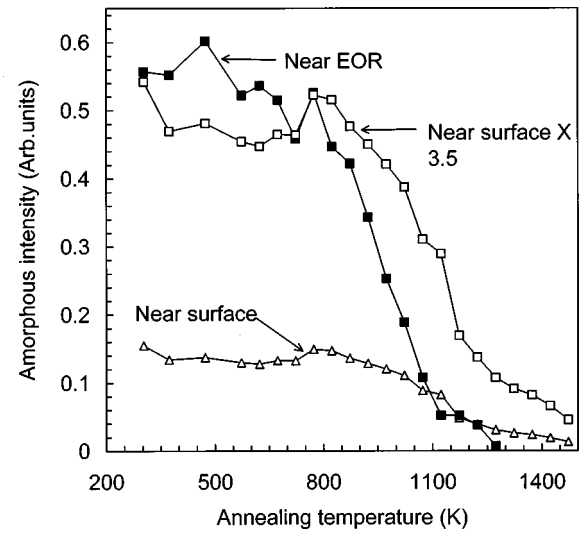

FIG. 13. Average amorphous intensity over the first 2 μm below implantation surface and at the end of range vs annealing temperature. The decrease in the intensity with annealing temperature shows that the diamond lattice is gradually restored as the sample is annealed to higher temperatures. Also shown is a plot of the near-surface intensity multiplied by a factor of 3.5. The similarity of the two curves indicates that the annealing behavior is similar for the end of range and near-surface damage.

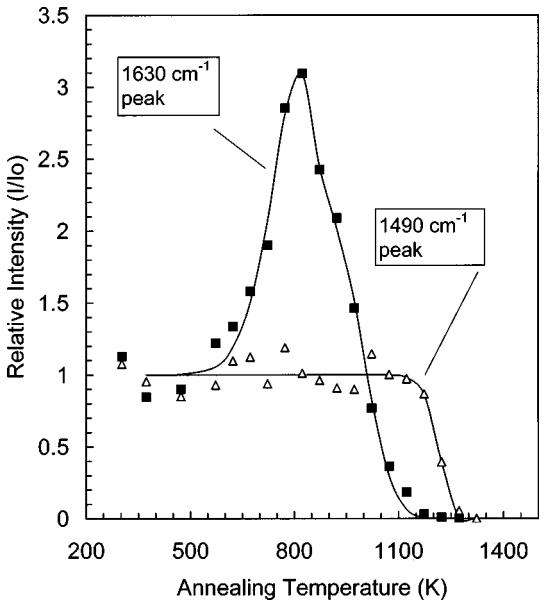

FIG. 14. Relative intensity of the 1490-cm^{-1} (open triangles) and 1630-cm^{-1} (solid squares) damage peaks vs annealing temperature at 2 μm below the implantation surface. The smooth curves are least-squares fit to the data points (see text for details).

After annealing at 1473 K, the amorphous fraction is reduced to about 10% of its initial value. These results show that annealing at up to 1473 K removes most of the damage, but is not enough to completely restore the diamond lattice. The remaining amorphous component is consistent with the observation that both the diamond peak shift and FWHM are not restored to their preimplantation values after annealing at up to 1473 K.

The results for the annealing of the EOR damage (i.e., a defect level of 1.1×10^{23} vac cm^{-3}) is remarkable. Despite the damage level being more than 10 times D_c near the end of range, the material nevertheless anneals back to diamond, and the amorphous fraction reduces to nearly zero for annealing temperatures in excess of 1300 K. It is seen from Fig. 13 that when the near-surface amorphous intensity is multiplied by a constant, the curve nearly overlays that for the end of range intensity, implying that the annealing behavior for both regions is the same. It is interesting to note that the EOR damage appears to have annealed somewhat more completely than the surface damage.

Figure 14 shows the intensity of the 1630- and 1490-cm^{-1} peaks as a function of annealing temperature for an initial defect density of 3.5×10^{21} vac cm^{-3} (taken at a depth of 2 μm below the implantation surface). The smooth curves are theoretical fits to the data points obtained by the method of least squares. The annealing behavior of the 1490-cm^{-1} peak was described by the differential equation of the form of Eq. (2) and the data points could be fitted with one decaying exponential similar to Eq. (6). The value of the activation energy for defect annealing, E_a, obtained from the fitting was 4.06 eV.

The non-monotonic dependence of the 1630-cm^{-1} peak intensity as a function of temperature indicates that two processes are involved: one in which the defect is formed (which occurs at about 650 K) and the other in which the defect is annealed (which occurs at about 1000 K). Because

of the initial growth observed in the annealing of the 1630-cm^{-1} peak, an additional term to Eq. (2) was required to describe the observed behavior. Thus we used the differential equation

$$\frac{dN}{dt} = r_a(N_f - N) - r_b N. \tag{9}$$

Equation (9) is a first-order differential equation, which can be solved as outlined in Sec. I C with $r_a = A_1 \exp(-E_1/k_BT)$ and $r_b = A_2 \exp(-E_2/k_BT)$. Here N_f in Eq. (9) is the maximum concentration of the defect responsible for 1630-cm^{-1} peak after a complete annealing of the unstable species, which aggregate to create it. Since N refers to the concentration of the defect at any time, the quantity $(N_f - N)$ represents the concentration, at any time, of the unstable species. By fitting the data points to the solution to Eq. (9), the activation energy for the growth of the defect was 0.55 eV, while a value of 1.22 eV was obtained for the annealing process. Once again, the 1490- and 1630-cm^{-1} peaks showing such markedly different annealing behavior is a clear indication that the defects which give rise to them are not of the same origin.

According to a recent publication by Prawer and Nugent,[23] a defect which fits the behavior of the 1630-cm^{-1} peak is the dumbbell defect or the ⟨100⟩ split interstitial, which consists of an isolated sp^2-bonded carbon pair occupying the position of one carbon atom in a normal diamond lattice. The dumbbell defect is the dominant stable defect which forms during ion irradiation.[24] The assignment of the 1630-cm^{-1} peak to the dumbbell defect is supported by the theoretical calculations by Drabold *et al.*[25] of the VDOS of a ta-C sample with 10% sp^2-bonded carbon content. In addition to revealing the existence of paired three fold-coordinated defects in the amorphous network, the calculations showed sharp localized modes at around 1600 cm^{-1} due to these paired sp^2-bonded carbon atoms. Furthermore, unpublished molecular dynamics results by Rosenblum and Prawer[26] show that the introduction of the split interstitial into an otherwise perfect diamond lattice gives rise to a peak in the VDOS at 1630 cm^{-1}.

The observed annealing behavior is also consistent with the assignment of the 1630-cm^{-1} peak to the dumbbell defect. The lower activation energy of 0.55 eV corresponds to the energy that the carbon self-interstitials require for mobility and to combine to form the split interstitial.[27] The higher activation energy corresponds to the energy required for the more stable split interstitial to migrate to sinks and annihilate or the energy required to break up the split interstitial back into self-interstitials. The initial rise in the intensity of the 1630-cm^{-1} defect peak suggests that the defect is formed from simpler defects which become mobile at lower temperatures and which combine to form the relatively stable split interstitial. The nonzero intensity of the peak in the as-implanted sample indicates that some of the defect is formed during the irradiation process. This can be explained by possible dynamic annealing which would not be unexpected under the implantation conditions employed, especially along the ion tracks. It is possible that the carbon self-interstitials, which are produced in large numbers during the irradiation process, are the building blocks for this defect. This view is supported by observing that an increase in damage in the unannealed sample towards the end of range is accompanied by an increase in the intensity of this peak. The increase in the intensity of the peak with damage is consistent with an increased availability of self-interstitials to form the defect. The bulk of these self-interstitials are created away from the regions of high thermal energy around the ion tracks and thus lack the energy to migrate and form the split interstitial. Upon heating to around 650 K, they become mobile and combine to form the split interstitial. At higher temperatures, when vacancies become mobile, the defect annihilates at the vacancy sites and disappears.

To speculate further on the structure of the defects that give rise to the 1490- and 1630-cm^{-1} peaks, a comparison is made with damage studies using absorption and electron paramagnetic resonance (EPR) techniques. Following radiation damage in type-II diamonds, the GR absorption series is observed. The lowest-energy peak of the series, the GR1, has a zero phonon line at 1.673 eV and is due to a neutral vacancy with an activation energy of 2.3 eV.[28] In addition, following irradiation, absorption bands with zero phonon lines at 4.582 and 1.86 eV, among others, are observed, as is a vibrational peak at 1570 cm^{-1}.

The band at 4.582 eV, referred to as the 5RL center, and the 1570-cm^{-1} vibrational peak result from a pair of carbon atoms, which fit the structure of a split interstitial.[29,30] The 5RL center and the 1570-cm^{-1} peak grow in intensity with increasing annealing temperature up to about 770 K, after which they diminish, annealing out in the range 920–1170 K.[30–32] The annealing behavior of these structures follows closely the results of the present study for the 1630-cm^{-1} Raman peak and may be explained similarly, lending strong support to our assignment of the 1630-cm^{-1} peak to a split interstitial.

The 1.86-eV absorption band is thought to be due to an interstitial with activation energy for annealing of 1.68 eV. Comparisons with EPR show that the 1.86-eV line correlates with the strength of the R2 EPR band,[33] the properties of which have recently been shown[31] to be consistent with those for a ⟨001⟩ split interstitial. R2 anneals out in the range 570–720 K.[34] Another EPR band, the R1, anneals out in the temperature range 600–700 K with an activation energy of 0.6 eV. The temperatures at which the R1 and R2 bands anneal out are too low compared to 1000 K, at which the 1630-cm^{-1} Raman peak, thought to be interstitial related, anneals out. They do, however, correspond to the temperature at which the 1630-cm^{-1} Raman peak intensity increases as a function of temperature. It may be, then, that the defects, which correspond to R1 and R2, combine to give rise to the dumbbell defect.

As mentioned above, the energy of the 1490-cm^{-1} peak lies midway between that corresponding to single sp^3-bonded carbon and sp^2-type double bonds, thus suggesting that the defect corresponds to a mixture of conjugated double and single bonds. The sharpness of the peak indicates that the defect responsible is very small and well defined. The most likely defect is a single vacancy or divacancy. In the vicinity of a vacancy, regions of mixed single and double bonds are formed. Rosenblum[26] has shown that, when a vacancy is introduced into an otherwise pristine diamond lattice, new vibrational modes appear at 1470 cm^{-1}. EPR data

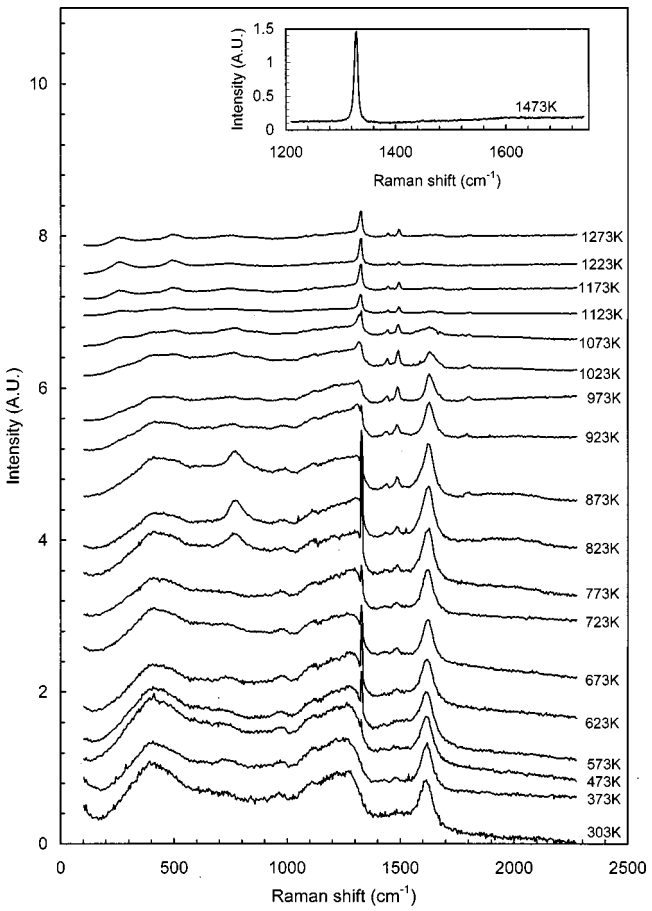

FIG. 15. Normalized Raman spectra acquired by the 514.5-nm line of an argon ion laser at the end of range of a diamond sample implanted with 1-MeV helium ions. Despite the end of range damage being well above the amorphization threshold, the inset shows that all the damage features have disappeared and only the first-order diamond Raman peak is left after annealing at 1470 K.

have also identified a vacancy-related center in radiation-damaged diamond. The center, referred to as R4/W6, anneals out at 1200 K and is though t to be a nearest-neighbor divacancy in the neutral charge state.[35] This annealing temperature is very close to 1223 K where the 1490-cm^{-1} Raman peak observed in the present study anneals. Thus the defect giving rise to the 1490-cm^{-1} peak may be composed of two nearest-neighbor vacancies.

D. Annealing of diamond irradiated well above D_c

Figure 15 shows the Raman spectra recorded as a function of annealing temperature for a cross-sectional point close to the end of range where the initial damage level is 1.1×10^{23} vac cm^{-3}. The spectra were recorded in the ''diamond-forbidden'' orientation, but without correction, so that the first-order diamond line is visible because of polarization breakthrough. In some of the spectra a very sharp first-order diamond line can be observed at 1330 cm^{-1}, which originates from the undamaged region beyond the end of range and is ignored in this discussion. The spectrum of the unannealed (303 K) sample is typical of that of amorphous material. No first-order diamond line is visible and the spectrum closely follows the VDOS of diamond.

The most dramatic and unexpected observation is the near-complete annealing of the diamond as is evidenced by the disappearance at the highest annealing temperatures (see the inset to Fig. 15) of all the defect peaks, the near restoration of the first-order diamond line to its preimplantation FWHM and position, and the near reduction to zero of the amorphous fraction (see Fig. 13). We note that annealing did not result in graphitization even at the end of range where the damage far exceeded D_c. This may be due to the large pressures to which the damage structures are subjected which constrain them from relaxing to graphite. Some damage still remains as is evidenced by the fact that the diamond FHWM is $\sim$6 cm^{-1} and the peak position is $\sim$1328 cm^{-1} (c.f. 3.01 and 1332.03 cm^{-1} for pristine diamond). It is conceivable that annealing to temperatures higher than the $\sim$1500 K employed here will result in total repair of the diamond lattice following deep damage.

In addition to the features already discussed, in the Raman spectra of Fig. 15, broad peaks are observed at 250, 480, and 750 cm^{-1}. The peaks at 250 and 480 cm^{-1} appear at around 1100 K, have their highest intensity at 1220 K, and decrease again at 1300 K. The peak at 750 cm^{-1} has its maximum intensity at about 873 K. (These features are also observed for damage levels well below D_c, but are less pronounced.) We cannot at present assign these peaks to particular defect structures; however, by changing the excitation wavelength from 514 to 488 nm, we were able to confirm that these peaks originate in Raman scattering and are not due to fluorescence.

In Fig. 15, the 1490-cm^{-1} peak and its associates, the 1430-, 1680-, and 1800-cm^{-1} peaks are virtually absent for the as-implanted sample (this is consistent with the dependence of this peak's intensity on damage as shown in Fig. 10). Between 400 and 600 K, only a small showing is recorded. From 600 K, the peaks gradually grow peaking at around 1000 K, after which they again begin to decrease in intensity for higher-temperature anneals. This observation and the damage-dependent behavior shown in Fig. 10 suggest that the vibrational modes arising from this vacancy-related defect are easily quenched in the vicinity of extensive damage. As damage is removed by annealing at progressively higher temperatures, there is a corresponding increase in the intensity of the peak because the removal of damage in the vicinity reduces the degree of quenching. However, above about 1100 K, the defect that gives rise to this peak becomes mobile and quickly anneals out, as is reflected in the diminishing size of the peak in Fig. 15.

IV. SUMMARY AND CONCLUSIONS

(i) The critical dose for amorphization, D_c, of diamond damaged by deep ion implantation is about 1×10^{22} vac cm^{-3}, the same value previously determined for shallow ion damage. The difference between shallow and deeply buried damage is that for the latter damage levels above D_c can be annealed, whereas in the former case annealing results in relaxation to graphite.

(ii) The annealing of the 1490-cm^{-1} peak obeys first-order kinetics and is characterized by one first-order process with an activation energy of 4.06 eV.

(iii) The annealing of the 1630-cm^{-1} peak follows first-

order kinetics characterized by two first-order processes with activation energies of 0.55 and 1.22 eV. The lower activation energy is attributed to the migration energy of simpler defects which combine to form the defect responsible for the 1630-cm^{-1} peak, while the higher activation energy corresponds to the migration energy of the defect that causes the 1630-cm^{-1} peak.

(iv) Based on the location of the defect peaks, their annealing behavior, and theoretical models, the 1490-cm^{-1} peak is assigned to a vacancy or divacancy with conjugated single and double bonds, while the 1630-cm^{-1} peak is attributed to the $\langle 100 \rangle$ split interstitial defect.

(v) The peak width and peak shift of both the first-order Raman line and the defect peaks are linearly related. The increase in width is due to a linear decrease in phonon lifetime with damage below the amorphization limit due to increased scattering and decay of the phonons. The shift to lower wave numbers of the peak positions is Kramers-Kronig related to the increase in linewidth. The first-order diamond peak symmetry suggests that the phonon decay is via simple scattering from point defects rather than phonon confinement.

(vi) The Raman spectrum shows signals which originate from amorphous zones even for the lowest damage levels studied, which are concomitant with signals from the first-order diamond line and from the divacancy and split interstitial. Note that the shape of the amorphous component, as seen from Fig. 6, does not change with increased damage. This implies that amorphous clusters and damaged, but still essentially single-crystalline, material coexist in the irradiated volume. The picture to emerge is then as follows: Radiation damage creates tiny amorphized regions along the ion tracks which are isolated and far apart for low levels of damage. Interspersed between the amorphous clusters are point defects in an otherwise largely damage-free diamond lattice. As the damage increases, the amorphized regions grow in size and in number. These changes are reflected in an increased intensity of the amorphous fraction with damage. At sufficiently high damage levels, the amorphized clusters overlap and the whole damaged region amorphizes. In this picture, the Raman spectra obtained in the ''diamond-allowed'' configuration come mainly from the regions between the amorphous clusters, which explains why the symmetry in the first-order diamond line persists even with increased damage. The ''diamond-forbidden'' spectra are a result of scattering from the amorphized damage clusters and the point defects. The Raman spectrum thus corresponds to the broadened diamond VDOS, although it retains its diamond characteristics with a cutoff frequency slightly higher than the zone center diamond mode.

(vii) In conclusion, the findings of this research hold important implications for the realization of chemical doping of diamond using ion implantation. Far greater care must be taken if shallow doping is intended to ensure that D_c is not exceeded. Because it is possible to anneal damage in excess of D_c for deeply buried damage, the latter offers some flexibility and would be ideal in cases where heavy doping is required. Our present and future work will now focus on applying the knowledge gained here to more practical systems such as correlating the intensity of the defects with conductivity of doped diamond samples.

ACKNOWLEDGMENTS

The authors gratefully acknowledge stimulating discussions with Professor R. Besserman of the Solid State Institute and Physics Department, Technion-Israel Institute of Technology, Haifa, Israel.

*Author to whom correspondence should be addressed. Email address: s.prawer@physics.unimelb.edu.au

[1] *The Properties of Natural and Synthetic Diamond*, edited by J. E. Field (Academic, New York, 1992).
[2] J. F. Prins, Mater. Sci. Rep. **7**, 271 (1992).
[3] D. S. Knight and W. B. White, J. Mater. Res. **4**, 385 (1989).
[4] W. N. Wang, N. A. Fox, P. W. May, M. P. Knapper, G. Meaden, P. G. Partridge, M. N. R. Ashfold, J. W. Steeds, I. P. Hayward, and G. D. Pitt, Phys. Status Solidi A **154**, 255 (1996).
[5] R. Walker, S. Prawer, D. N. Jamieson, and K. W. Nugent, Appl. Phys. Lett. **71**, 1492 (1997).
[6] J. F. Ziegler, J. P. Biersack, and U. Littmark, *The Stopping and Range of Ions in Solids* (Pergamon, New York, 1985).
[7] M. S. Dresselhaus and R. Kalish, *Ion Implantation in Diamond, Graphite and Related Materials* (Springer-Verlag, Berlin, 1992).
[8] J. F. Prins, Mater. Sci. Rep. **7**, 271 (1992).
[9] G. Davies, *Properties and Growth of Diamond* (INSPEC, London, 1994).
[10] R. Kalish and S. Prawer, in *Handbook of Industrial Diamonds and Diamond Films*, edited by M. A. Prelas, G. Popovici, and L. K. Bigelow (Dekker, New York, 1997), pp. 945–982.
[11] R. Kalish, in *The Physics of Diamond*, Proceedings of The International School of Physics ''Enrico Fermi,'' Course CXXXV, Varenna, 1997, edited by A. Paoletti and A. Tucciarone (IOS Press, Amsterdam, 1997), pp. 373–409.
[12] C. Uzan-Saguy, V. Richter, S. Prawer, Y. Lifshitz, E. Grossman, and R. Kalish, Appl. Phys. Lett. **67**, 1194 (1995).
[13] F. F. Morehead, Jr. and B. L. Crowder, Radiat. Eff. **6**, 27 (1970).
[14] R. Kalish and S. Prawer, Phys. Rev. B **51**, 15 711 (1995).
[15] X. Huang, F. Ninio, L. J. Brown, and S. Prawer, J. Appl. Phys. **77**, 5910 (1995).
[16] R. Shucker and R. W. Gammon, Phys. Rev. Lett. **25**, 222 (1970).
[17] J. Bourgoin and M. Lanoo, *Point Defects in Semiconductors II, Experimental Aspects* (Springer-Verlag, Berlin, 1983).
[18] J. O. Orwa, Ph.D. thesis, The University of Melbourne, 1999.
[19] D. N. Jamieson, S. Prawer, K. W. Nugent, and S. P. Dooley, Nucl. Instrum. Methods Phys. Res. B **106**, 641 (1995).
[20] M. S. Liu, L. Bursill, S. Prawer, and R. Besserman, Phys. Rev. B **61**, 3391 (2000).
[21] S. Prawer, K. W. Nugent, and D. N. Jamieson, Diamond Relat. Mater. **7**, 106 (1998).
[22] C. Z. Wang and K. M. Ho, Phys. Rev. Lett. **71**, 1184 (1993).
[23] S. Prawer and K. W. Nugent, in *Amorphous Carbon: State of the Art*, edited by S. R. P. Silva, J. Robertson, W. I. Milne, and G. A. J. Amaratunga (World Scientific, Singapore, 1997), p. 199.
[24] R. Kalish, A. Reznik, S. Prawer, D. Saada, and J. Adler, Phys. Status Solidi A **174**, 83 (1999).
[25] D. A. Drabold, P. A. Fedders, and P. Stumm, Phys. Rev. B **49**, 16 415 (1994).
[26] R. Rosenblum and S. Prawer (private communication).

[27] D. G. McCulloch and S. Prawer, J. Appl. Phys. **78**, 3040 (1995).
[28] L. Allers, A. T. Collins, and J. Hiscock, Diamond Relat. Mater. **7**, 228 (1998).
[29] A. T. Collins and P. M. Spear, J. Phys. C **19**, 6845 (1986).
[30] Y. Nisida, Y. Yamada, H. Kanda, T. Nakashima, S. Sato, S. Kobayashi, and M. Okada, in *Defects in Insulating Materials*, edited by O. Kanert and J. M. Spaeth (World Scientific, Singapore, 1993), p. 496.
[31] A. T. Collins, Diamond Relat. Mater. **8**, 1455 (1999).
[32] G. S. Woods, Philos. Mag. B **50**, 673 (1984).
[33] J. Walker, Rep. Prog. Phys. **42**, 1605 (1979).
[34] D. Twitchen, Ph.D. thesis, University of Oxford, 1997.
[35] D. Twitchen, M. E. Newton, M. E. Baker, T. R. Anthony, and W. F. Banholzer, Phys. Rev. B **59**, 12 900 (1999).